© 2014. Published by The Company of Biologists Ltd | The Journal of Experimental Biology (2014) 217, 3898-3909 doi:10.1242/jeb.084897

RESEARCH ARTICLE

Clap and fling mechanism with interacting porous wings in tiny insect flight

Arvind Santhanakrishnan[1], Alice K. Robinson[2], Shannon Jones[3], Audrey Ann Low[4], Sneha Gadi[4], Tyson L. Hedrick[3] and Laura A. Miller[3,4,*]

ABSTRACT

The aerodynamics of flapping flight for the smallest insects such as thrips is often characterized by a 'clap and fling' of the wings at the end of the upstroke and the beginning of the downstroke. These insects fly at Reynolds numbers (*Re*) of the order of 10 or less where viscous effects are significant. Although this wing motion is known to augment the lift generated during flight, the drag required to fling the wings apart at this scale is an order of magnitude larger than the corresponding force acting on a single wing. As the opposing forces acting normal to each wing nearly cancel during the fling, these large forces do not have a clear aerodynamic benefit. If flight efficiency is defined as the ratio of lift to drag, the clap and fling motion dramatically reduces efficiency relative to the case of wings that do not aerodynamically interact. In this paper, the effect of a bristled wing characteristic of many of these insects was investigated using computational fluid dynamics. We performed 2D numerical simulations using a porous version of the immersed boundary method. Given the computational complexity involved in modeling flow through exact descriptions of bristled wings, the wing was modeled as a homogeneous porous layer as a first approximation. High-speed video recordings of free-flying thrips in take-off flight were captured in the laboratory, and an analysis of the wing kinematics was performed. This information was used for the estimation of input parameters for the simulations. Compared with a solid wing (without bristles), the results of the study show that the porous nature of the wings contributes largely to drag reduction across the *Re* range explored. The aerodynamic efficiency, calculated as the ratio of lift to drag coefficients, was larger for some porosities when compared with solid wings.

KEY WORDS: Thrips, Aerodynamics, Flapping flight, Wing kinematics, Locomotion, Weis Fogh mechanism, Bristled wing, Fringed wing, Immersed boundary method

INTRODUCTION

Though hard to notice even when they hop, walk or fly, the smallest flying insects reported in the literature (with body lengths less than 1 mm) are of considerable ecological and agricultural importance. For example, over 5500 species of thrips have been described thus far (Morse and Hoddle, 2006). They function in multiple important roles such as: (1) effective transmitters of pollen during feeding (Terry, 2001; Terry, 2002), (2) invasive pests of agriculturally important plants (Crespi et al., 1997; Palmer et al., 1990) and (3) biological vectors of microbial plant pathogens such as Tospoviruses (Ullman et al., 2002; Jones, 2005). Parasitoid wasps consist of a dozen hymenopteran superfamilies that include some of the smallest insects, such as *Mymar* sp. These insects have received much attention in recent years because of their potential as a natural control of agricultural pests (Austin and Dowton, 2000). Understanding the aerodynamics of flapping flight in these tiny insects provides a means of exploring their dispersal strategies and ranges; it may also help us to elucidate the principles of active flight in some of the smallest animals (Lewis, 1964; Lewis, 1965).

Although many researchers have investigated the complex nature of the aerodynamics of flapping flight in insects ranging from the scale of the hawk moth *Manduca sexta* (Usherwood and Ellington, 2002; Wang, 2005; Hedrick et al., 2009) to the fruit fly *Drosophila* (Vogel, 1962; Dickinson and Götz, 1993; Dickinson et al., 1999), the aerodynamics of flight in the smallest insects remains relatively unexplored (Horridge, 1956; Weis-Fogh, 1973; Ellington, 1980; Miller and Peskin, 2009). The Reynolds number (*Re*) is commonly used to quantify the ratio of inertial to viscous effects in a fluid and is given as $Re=\rho LU/\mu$ where ρ is the density of air, μ is the dynamic viscosity of air, L is the chord length of the wing and U is the wing tip velocity. *Drosophila* and *Manduca* span the *Re* range from about 100 to 1000, while some of the smallest thrips and parasitoid wasps fly at $Re<10$.

It appears that one of the predominant lift-augmenting mechanisms for nearly all insects is flight at high angles of attack (~45 deg). The resulting high lift is possibly due to the presence of a stable leading edge vortex, which remains attached to the upper surface of the wing until stroke reversal (Ellington et al., 1996; van den Berg and Ellington, 1997a; van den Berg and Ellington, 1997b; Liu et al., 1998; Usherwood and Ellington, 2002; Birch and Dickinson, 2003; Birch et al., 2004). This vortex creates a negative pressure region above the wing and enhances lift. Lift is also generated when the trailing edge vortex (also known as the starting vortex) is shed from the wing and consequently induces circulation around the wing. 'Wake capture' could also enhance lift as the wing moves back through its wake due in part to the fact that the velocity of the fluid relative to the wing is increased (Wang, 2000).

Flight aerodynamics and wing kinematics for the smallest insects differ from those of larger animals such as *Drosophila* species. Horridge (Horridge, 1956) proposed that tiny insects employ an asymmetric flight stroke via adjusting the angle of attack differentially such that most of the lift is generated during the downstroke and negative lift is minimized during the upstroke. Weis-Fogh (Weis-Fogh, 1973) analyzed video recordings capturing the hovering flight of the tiny parasitic wasp *Encarsia formosa* and discovered the use of a 'clap and fling' mechanism. More specifically, the wings were observed to clap together at the end of each upstroke and fling apart

[1]School of Mechanical & Aerospace Engineering, Oklahoma State University, 218 Engineering North, Stillwater, OK 74078-5016, USA. [2]University of California, Irvine, Irvine, CA 92697, USA. [3]Department of Biology, University of North Carolina, Chapel Hill, NC 27599, USA. [4]Department of Mathematics, University of North Carolina, Chapel Hill, NC 27599, USA.

*Author for correspondence (lam9@email.unc.edu)

Received 16 May 2013; Accepted 20 August 2014

The Journal of Experimental Biology

The Journal of Experimental Biology (2014) doi:10.1242/jeb.084897

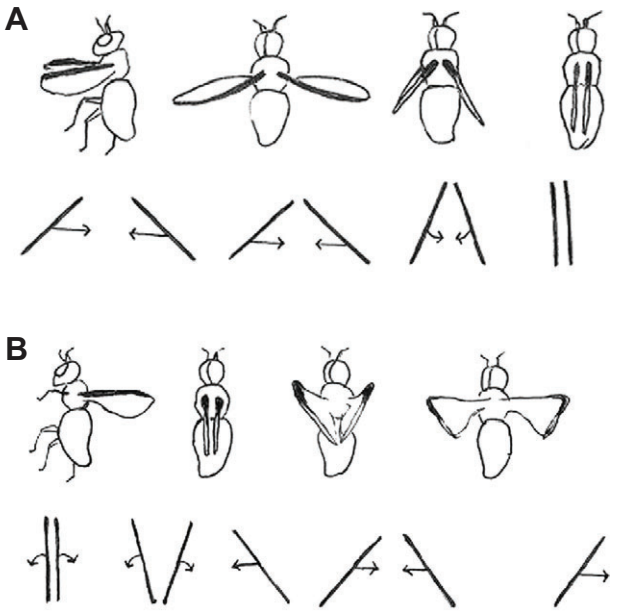

Fig. 1. Diagram showing a two-dimensional simplified 'clap and fling'. Taken from Miller and Peskin (Miller and Peskin, 2005). Top: the three-dimensional motion of the insect. Bottom: the corresponding two-dimensional approximation. (A) At the beginning of the upstroke, the wings rotate together about the leading edges to perform the clap. (B) At the beginning of the downstroke, the wings rotate apart about the trailing edges to perform the fling.

at the beginning of each downstroke (see Fig. 1). The fling motion is produced by a rotation of the wings about the common trailing edge, during which time a pair of large leading edge vortices are formed (Maxworthy, 1979). Lighthill (Lighthill, 1973) analytically showed that the clap and fling mechanism could be used for lift augmentation even in 2D inviscid flows. The clap and fling mechanism has since been observed in other insects such as *Thrips physapus* (Ellington, 1980; Ellington, 1984), the parasitoid wasps *Muscidifurax raptor* and *Nasonia vitripennis* (Miller and Peskin, 2009), the greenhouse white-fly *Trialeurodes vaporariorum* (Weis-Fogh, 1975) and some butterflies (Srygley and Thomas, 2002). It is also commonly observed in the tethered flight of larger insects such as *Drosophila* species (Vogel, 1967).

In addition to measurements of tiny insects in free flight, computational fluid dynamics has been used to explore the force generation and resulting flow structures produced during the flight of tiny insects. Here, we describe the dimensionless force coefficients as follows:

$$C_{\mathrm{L}} = \frac{2F_{\mathrm{L}}}{\rho S U}, \quad (1)$$

$$C_{\mathrm{D}} = \frac{2F_{\mathrm{D}}}{\rho S U}, \quad (2)$$

where C_{L} is the lift coefficient, C_{D} is the drag coefficient, U is the constant characteristic velocity, F_{L} describes the lift or vertical component of the force acting against gravity, F_{D} describes the drag or horizontal component of the force and S is the surface area of the wing. Note that the characteristic velocity, U, does not change in time so that the force coefficients are functions of time. Another way to think about C_{L} and C_{D} is to consider them as dimensionless forces. Numerical simulations of flapping wings have shown that lift coefficients are reduced and drag coefficients are increased

Fig. 2. Images showing some of the variation in the number and spacing of bristles present in the wings of tiny insects. (A) The bristled wing of an adult female parasitoid wasp *Mymar* sp. from New Zealand (courtesy of S. E. Thorpe). (B) The bristled wings of an adult thrips collected in Chapel Hill, NC, USA.

significantly when the *Re* is lowered from 100 to 20 or below (Wang, 2000; Miller and Peskin, 2004; Wu and Mao, 2004). Numerical simulations of clap and fling show that lift coefficients can be enhanced by almost 100% for *Re* in the range of the smallest insects (Mao and Xin, 2003; Miller and Peskin, 2005; Kolomenskiy et al., 2010). The cost of clap and fling for small insects ($Re \approx 10$) is that the drag required to fling the wings apart may be an order of magnitude larger than the force required to move a single wing with the same motion (Miller and Peskin, 2009). As the opposing drag forces on each wing nearly cancel during the fling, these large forces do not have a clear aerodynamic benefit.

The previous experimental and computational work has focused on models of solid wings, but the wings of many small insects such as thrips are fringed or bristled rather than continuous (Ellington, 1980) (see Fig. 2). The aerodynamic benefits of this type of wing are not clear. Sunada et al. (Sunada et al., 2002) constructed a

dynamically scaled model of a thrips wing and measured lift and drag generated during single wing translation and rotation. Their results showed that lift and drag scaled proportionally with the addition of bristles, and they did not find a clear aerodynamic benefit. As the forces generated during the fling are up to an order of magnitude greater than the single wing case, it is possible that large differences in bristled wing aerodynamics may be seen when the wing–wing interaction is considered. The amount of airflow between the bristles is proportional to the normal force or pressure difference across the wing, and this effect could potentially result in significant airflow through the wings when forces are large.

In this study, a porous version of the immersed boundary was used to investigate the aerodynamics of bristled wings during clap and fling. Recordings of thrips in free take-off flight were filmed in the laboratory using high-speed videography. Kinematic analyses were performed, and the results were used to select input parameters for the simulations. Given the computational difficulty of resolving the flow through dozens of bristles in three dimensions, the wings were approximated to be homogeneous porous layers in two dimensions. Lift and drag coefficients were calculated as functions of time during the flapping cycle. Parametric studies were performed to compare the aerodynamics of solid wings and bristled wings with several levels of porosity for $Re \leq 10$.

RESULTS

Kinematic observations

Snapshots taken during the clap and fling wingbeat of a typical thrips in free take-off flight are shown in Fig. 3. The images were recorded at 4000 frames s^{-1}. Note the characteristic bristled wing form. At the end of the upstroke (the clap), the wings are raised normal to the body axis and come within about 1/6 to 1/10 chord lengths of each other. This clap motion is characterized by a simultaneous rotation of the wing about the base and the trailing edge. At the beginning of the downstroke (the fling), the wings rotate simultaneously about the trailing edge and the wing base, which results in the fling motion. Videos of typical thrips in take-off flight are shown in supplementary material Movies 1–3.

Four of the videos collected showed thrips that ceased to flap their wings shortly after take-off. During this time, the insects spread their wings and passively floated downward. This behavior is termed ‘parachuting’ herein rather than ‘gliding’, using the convention given by Alexander (Alexander, 2003). Parachuting refers to the use of drag-producing structures in order to reduce the speed of falling. Gliding, in contrast, relies on lift production. To make an operational distinction between the two, maneuvers using descent angles lower than 45 deg are considered to be gliding maneuvers and above 45 deg are considered to be parachuting maneuvers. In all cases, the descent angles for parachuting thrips were greater than 45 deg (e.g. the thrips were not gliding). Snapshots taken during a typical parachuting maneuver are shown in Fig. 4. In this case, the thrips spreads its four wings above its body about 8 wingbeats after take-off. The insect then passively parachutes downward until it is out of the field of view of the camera. Supplementary material Movie 4 shows a video of this maneuver.

Wing tip speed as a function of time for two representative thrips is shown in Fig. 5. The two forewings were tracked over three strokes using DLTdv5 software (Hedrick, 2008) and velocities were measured via direct numeric differentiation. Maximum wing tip velocities are of the order of 1.5 m s^{-1}. The average flapping frequency measured for eight individuals (and a total of 45 wing strokes) was 254±32 Hz. A paired two sample *t*-test shows that the duration of the average upstroke (1.87±0.27 ms) was significantly shorter than that of the average downstroke (2.13±0.47 ms; P=0.00254). The length of the wings (base to tip) was 0.644±0.193 mm (N=6). If we assume an aspect ratio of about 2 (see Fig. 2), this results in a Reynolds number of about 14 based upon the average wing tip velocity and a total sweep of 120 deg. Looking at the smallest (0.383 mm span) to largest (1.03 mm span) individual gives a Re range of 4.9–35.

Mathematical modeling

The complex structure of the bristled wing prevalent in tiny insects such as thrips is modeled herein as a porous layer using a previously derived method (Kim and Peskin, 2006; Stockie, 2009). Permeability is incorporated into the immersed boundary method using an interpretation of Darcy’s law, which states that the relative velocity of a fluid through a porous medium is proportional to the pressure difference across the boundary:

$$\dot{Q} = \frac{-\kappa A_{\mathrm{p}} [p]}{\mu T_{\mathrm{p}}}, \tag{3}$$

where $\dot{Q}$ is the volumetric flow rate, κ is the permeability of the layer (with units of m^2), $[p]$ is the pressure difference across the layer, T_{p} is the thickness of the layer, A_{p} is the surface area of the layer and μ is the viscosity of the fluid.

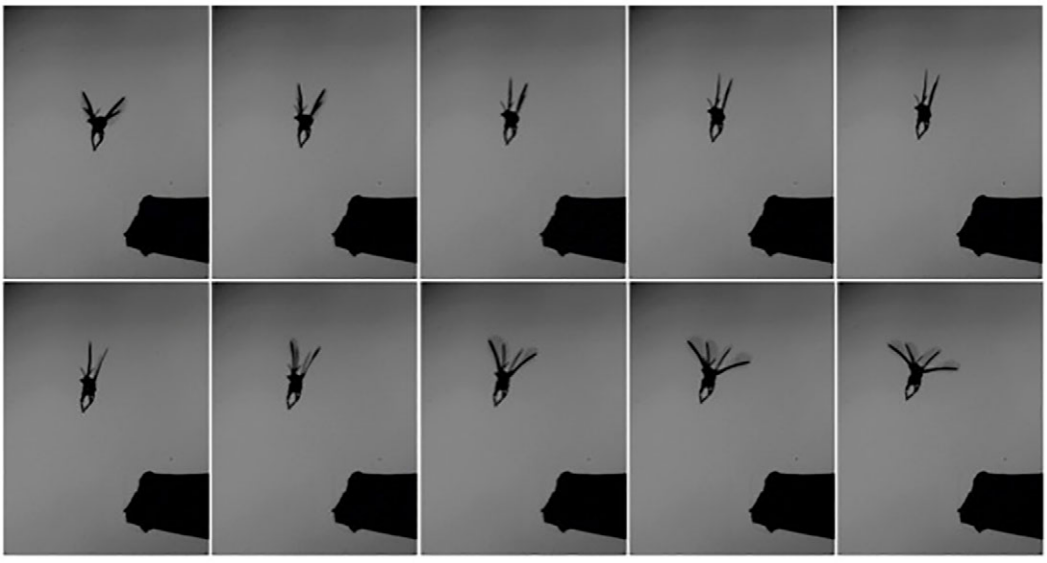

Fig. 3. Successive snapshots taken during clap and fling of a thrips in free take-off flight. The images were recorded at 4000 frames s^{-1}. Note the characteristic bristled wing form. Top: at the end of the upstroke, the wings are raised vertically with respect to the body and come within about 1/6 to 1/10 chord lengths of each other. Bottom: at the beginning of the downstroke, the wings rotate about the trailing edge and the root performing the fling motion.

The Journal of Experimental Biology (2014) doi:10.1242/jeb.084897

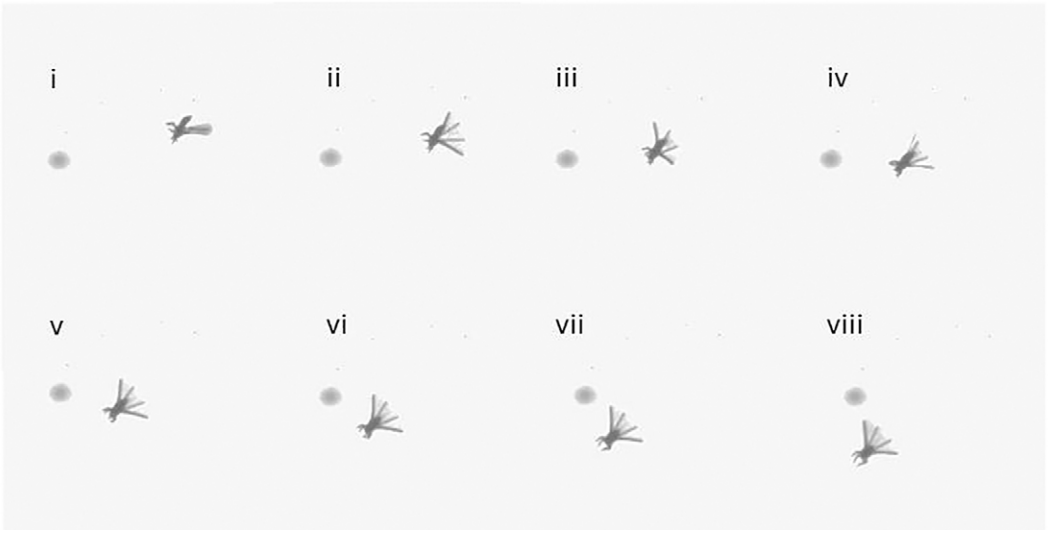

Fig. 4. A passive 'parachuting' maneuver from a video recording at 4000 frames s^{-1}. Snapshots were taken every 1.25 ms about eight wingbeats after take-off. The wings clapped together at the beginning of the downstroke (i). Rather than completing the stroke, the thrips spreads its wings (ii–v) and passively parachutes downward until it leaves the field of view (vi–viii).

Equating the volumetric flow rate to the difference between the local fluid velocity and the velocity of the boundary results in an expression for the slip between the boundary and fluid. This is incorporated into the immersed boundary method by modifying the velocity of the boundary. Rather than moving the boundary at the local fluid velocity, a slip is used that is proportional to the force per unit area acting normal to the boundary (which is equivalent to the pressure jump) and the porosity. The velocity of boundary motion is modified as follows:

$$\mathbf{X}_t(q,t) = \mathbf{U}(q,t) + \Lambda\left(\mathbf{F}(q,t)\cdot\mathbf{n}\right)\mathbf{n}\,, \tag{4}$$

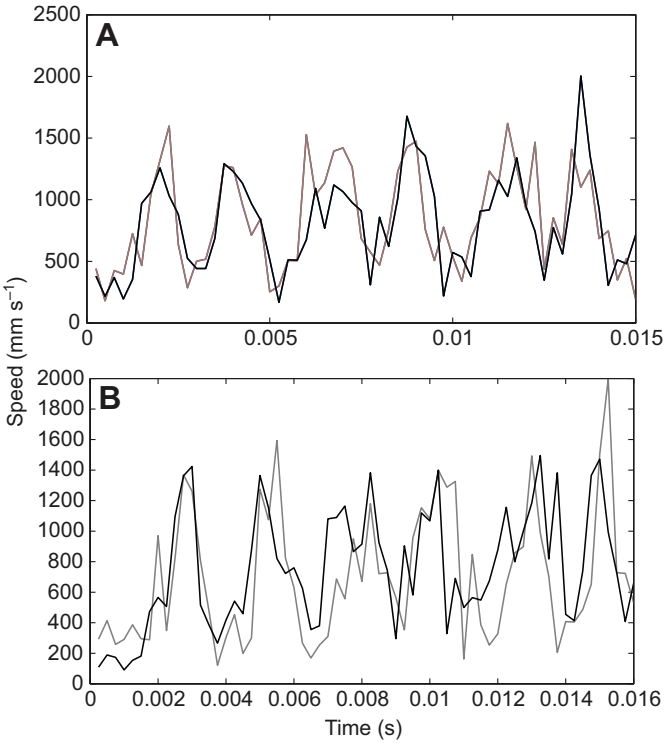

Fig. 5. Wing tip speed of the left and right wing tips as a function of time. Data for two representative thrips are shown. Black, left wing; gray, right wing. Maximum wing tip velocities are of the order of 1.5 m s^{-1}. Flapping frequencies are of the order of 250 Hz, and the upstroke was significantly shorter than the downstroke.

where $\mathbf{X}(q,t)$ gives the Cartesian coordinates of the boundary point labeled by the Lagrangian parameter q at time t, $\mathbf{U}$ is the velocity of the boundary at position q, $\mathbf{F}(q,t)$ is the force per unit length applied by the boundary to the fluid as a function of the Lagrangian position q and the time t, $\mathbf{n}$ is the unit vector normal to the boundary and Λ is a proportionality constant termed the porosity (see Kim and Peskin, 2006) and has units of m^2 (N s)$^{-1}$. The physical interpretation of the porosity coefficient, Λ, is that it is equal to the number of pores in an interval multiplied by the conductance of the material per unit arc length. The relationship between the porosity, Λ, and the permeability, κ, is given by $\Lambda=\kappa/(A_p\mu)$.

Relating the porosity to the leakiness

Another metric that has been used to measure the permeability of a structure is the leakiness, $\bar{L}$ (Cheer and Koehl, 1987). $\bar{L}$ is calculated as the ratio of the actual flux through the structure over the flux in the inviscid (μ=0) case:

$$\bar{L} = \frac{\dot{Q}}{UA_p}\,, \tag{5}$$

where U is the freestream velocity and $\dot{Q}$ is the volumetric flow rate. Note that there is no flow through the porous structure when $\bar{L}$=0, and the flow is inviscid when $\bar{L}$=1. The leakiness of thrips wings and other bristled appendages can be estimated using the analytical results of Cheer and Koehl (Cheer and Koehl, 1987). These results have also been experimentally validated by Loudon et al. (Loudon et al., 1994). Thrips have a cylinder diameter to gap ratio of 1:10 and 1:12 at a bristle-based Re of 1.0×10^{-2} (Ellington, 1980). This leads to leakiness values ranging from about 0.15 to 0.24.

The porosity, Λ, used by Kim and Peskin can be directly related to the leakiness, $\bar{L}$, using an appropriate non-dimensionalization. The leakiness is calculated at steady state for cylinders arranged normal to the direction of flow. If one divides the porosity by the steady-state force per unit area at a 90 deg angle of attack, $\bar{F}$, over the free stream velocity, U, the result is the percentage slip between the boundary and the fluid:

$$\mathrm{Le} = \frac{\Lambda U}{\bar{F}}\,, \tag{6}$$

where Le is the dimensionless porosity. When the boundary moves normal to the direction flow at steady state, Le is equivalent to the leakiness defined by Cheer and Koehl (Cheer and Koehl, 1987).

The Journal of Experimental Biology (2014) doi:10.1242/jeb.084897

This relationship uses the fact that the pressure jump across the porous boundary is equal to the normal force per area acting on the boundary, as described in Kim and Peskin (Kim and Peskin, 2006). The choice of characteristic force per unit area used in this study was $\bar{F}=1/2C_D\rho U^2$, where C_D was set to 6 (the approximate drag coefficient of a Re=10 wing at a 90 deg angle of attack). Leakiness is then maximized when the wing moves with a 90 deg angle of attack and would drop to zero at a 0 deg angle of attack (no flow in the tangential direction). In the simulations that follow, the effective leakiness varies in time as the normal force acting on the boundary changes over time due to wing–wing interactions, acceleration and changes in angle of attack. Throughout the remainder of the paper we will refer to the dimensionless porosity, Le, as the leakiness.

Table 1 shows all parameter values used in the simulations. For easy comparison with thrips and other insects, all simulation parameters are dimensionless using the following relationships:

$$\tilde{x}=\frac{x}{L}, \quad (7)$$

$$\tilde{t}=\frac{t}{L/U}, \quad (8)$$

$$\tilde{u}=\frac{u}{U}, \quad (9)$$

$$\tilde{k}_{\text{targ}}=\frac{k_{\text{targ}}}{\rho L U^2}, \quad (10)$$

where u is any component of the velocity field and tildes are used to denote the dimensionless parameter. Re was varied from 4 to 10 to span the range of tiny insects from the smallest parasitoid wasps to thrips. Re was adjusted by keeping all length and velocity scales constant and changing the dynamic viscosity appropriately. Le was varied from 0 (solid wing) to 0.28.

Description of prescribed kinematics

The simplified flight kinematics of clap and fling used in this paper are similar to those used in a number of experimental, analytical and computational papers (Lighthill, 1973; Bennett, 1977; Spedding and Maxworthy, 1986; Mao and Xin, 2003; Miller and Peskin, 2005). The translational and angular velocities during each half stroke were constructed using a series of equations to describe each part of the stroke as described previously (Miller and Peskin, 2009). For the case of clap, the wings translate towards each other at a constant rate at a constant 45 deg angle of attack. Deceleration and wing rotation then begin simultaneously at the end of the stroke. The wings rotate about the leading edges from 45 to 90 deg. For the case of fling, the wings rotate apart about the trailing edges from a 90 to a 45 deg angle of attack. Translation begins halfway during wing rotation. At the end of the translational acceleration phase, the wings continue to translate apart at a constant speed and a constant 45 deg angle of attack. Plots of translational and angular velocities as functions of time are shown in Fig. 6.

Table 1. Parameter values used in the simulations

Dimensionless parameters	Symbol	Value
Chord length	L	1
Domain length	D	20
Reynolds number	Re	4–10
Dimensionless porosity (leakiness)	Le	0–0.28
Spatial step size	dx	0.039
Time step size	dt	2.4×10^{-5}
Maximum translational velocity	U_{max}	1
Maximum rotational velocity	Ω_{max}	9.0
Target stiffness	k_{targ}	144

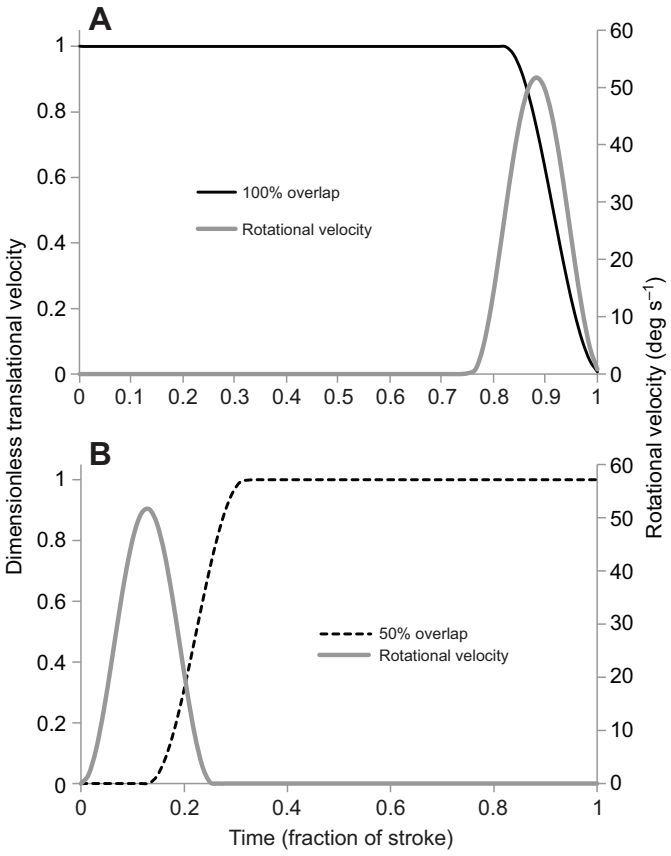

Fig. 6. Dimensionless translational and rotational velocities of the computational wings as functions of dimensionless time. (A) Kinematics for the clap with 100% overlap between translation and rotation at the end of the stroke. (B) Kinematics for the fling with 50% overlap between the beginning of rotation and the subsequent beginning of wing translation.

Either a single clap upstroke or a single fling downstroke was simulated. This simplification was made because the influence of the wake produced by the previous stroke is small for Re<10. The right wing was the mirror image of the left wing at all times during its motion. At the end of the upstroke and the beginning of the downstroke, the wings were placed 1/10 chord lengths apart unless otherwise noted.

Validation of method and choice of kinematics

The use of the immersed boundary to study clap and fling with solid wings has been previously validated through a convergence study and comparison with published experimental results (Miller and Peskin, 2005). A convergence study for a porous wing performing a fling at Re and leakiness values relevant to thrips was also carried out. Fig. 7 shows lift and drag coefficients as functions of time (fraction of stroke) for a 630×630 and a 1230×1230 grid with a leakiness value of Le=2.3×10^{-1}. The initial peaks correspond to the forces generated during the fling. Deviations in peak drag between the finer and coarser grids are due to differences in the effective width (and hence the gap) between the wings. A single immersed boundary point interacts with the fluid like a sphere with radius 1.255 grid cells (Bringley and Peskin, 2008). As a result, the wings have an effective width of about 2.51 grid cells, and the width of the wings is refined as the grid is refined. For the 630×630 grid, the

The Journal of Experimental Biology (2014) doi:10.1242/jeb.084897

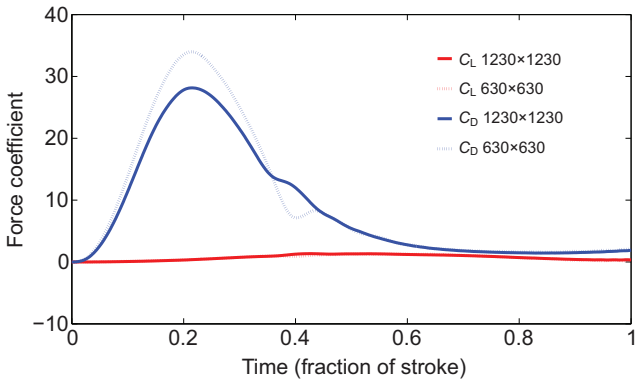

Fig. 7. Lift and drag coefficients (C_L and C_D) as a function of time (fraction of stroke) for a 630×630 and a 1230×1230 grid with a leakiness value of Le=2.3×10^{-1}. Deviations in peak drag are due to differences in the effective width (and hence the gap) between the wings. For the 630×630 grid, the effect gap size is 1.6% of the chord, and for the 1230×1230 grid, the effective gap size is 5.8% of the chord. Once the wings are sufficiently far apart, there is excellent agreement.

effect gap size is 1.6% of the chord, and for the 1230×1230 grid, the effective gap size is 5.8% of the chord. Once the wings are sufficiently far apart, there is excellent agreement.

During flight, the distance between the wings at the beginning of the fling varies from about 1/4 to 1/10 of the chord length. For example, Fig. 3 shows a gap of about 1/10 of the chord length. To determine the effect of the initial gap, the distances (measured from the middle of each wing) were varied from 1/10 to 1/2 of the chord length. The fact that the wings do not completely touch is fortuitous with regard to the immersed boundary method as the level of mesh refinement required scales inversely with the distance between the wings, and strictly speaking the method does not allow one to resolve the case of wings that are in direct contact. A method that can resolve wing contact for the case of solid rigid wings performing clap and fling has been described by Kolomenskiy et al. (Kolomenskiy et al., 2010; Kolomenskiy et al., 2011), and their results show larger lift as the distance between the wings approaches zero.

The choice of wing kinematics for the translation phase of the simulations is idealized. We were not able to quantitatively analyze angle of attack or stroke plane angle. Given the size of the thrips (~1 mm) and the wingbeat frequency (200–250 Hz), lighting and the plane of focus are significant challenges in terms of the amount of quantitative data that can be obtained. Another challenge is that the thrips are constantly changing their orientation and are susceptible to even the smallest breeze in the room. Without a clear measurement of flight direction and orientation, it is not possible to calculate stroke plane angle and angle of attack. The translation portion of the stroke was chosen so as to provide the maximum lift at a 45 deg angle of attack. As this study is mainly focused on what happens during the initial part of the fling, the kinematics of the translational portion is not significant to the major findings.

Single wing studies

Single wing studies were performed by placing a porous wing in a moving fluid. Parabolic flow with maximum velocity U_{max} was driven within a computational channel and upstream of the model wing by applying an external force, $\mathbf{f}'_{ext}$, to the fluid proportional to the difference between the desired fluid velocity and the actual fluid velocity, as described elsewhere (Miller et al., 2012). The difference between the actual and desired velocities was controlled with a 'stiffness' parameter, $k_{ext}=10k_{targ}$ (where k_{targ} is the target stiffness), such that the difference between the two velocities was always less than 0.1%.

Lift and drag coefficients as functions of time for fixed porous wings at a 45 deg angle of attack at *Re*=10 are shown in Fig. 8. The wing was fixed in place, and the background flow was ramped from zero to the characteristic velocity at t'=0.2. Maximum lift coefficients of 1.7 were achieved when the porosity was set to zero, which is equivalent to a solid wing. Lift did not significantly drop for leakiness values up to 10^{-1}. Maximum drag coefficients of about 3.4 were also found when the porosity was set to zero and also did not drop considerably.

Clap and fling

Drag coefficients as a function of time (fraction of stroke) for *Re*=10 are shown in Fig. 9 for a single clap and a single fling. Note that Le=0 corresponds to a solid wing. Four leakiness values ranging from 2.8×10^{-4} (least leaky) to 2.3×10^{-1} (most leaky) were examined. For the clap, the wings accelerate towards each other during the first 20% of the stroke. The forces plateau until the end of the stroke as the wings begin to rotated and clap together. For the clap, the peak in the drag coefficients at the end of the stroke corresponds to the large forces required to clap the wings together at low *Re* (Fig. 9A). For the fling, the initial large peak in the drag coefficients corresponds to the large forces required to fling the wings apart in a viscous fluid (Fig. 9B). The drag coefficients then plateau as the wings translate apart. The peak drag is lowered for the porous case compared with the solid case, and this drag-reducing effect increases rapidly for Le>2.8×10^{-4}.

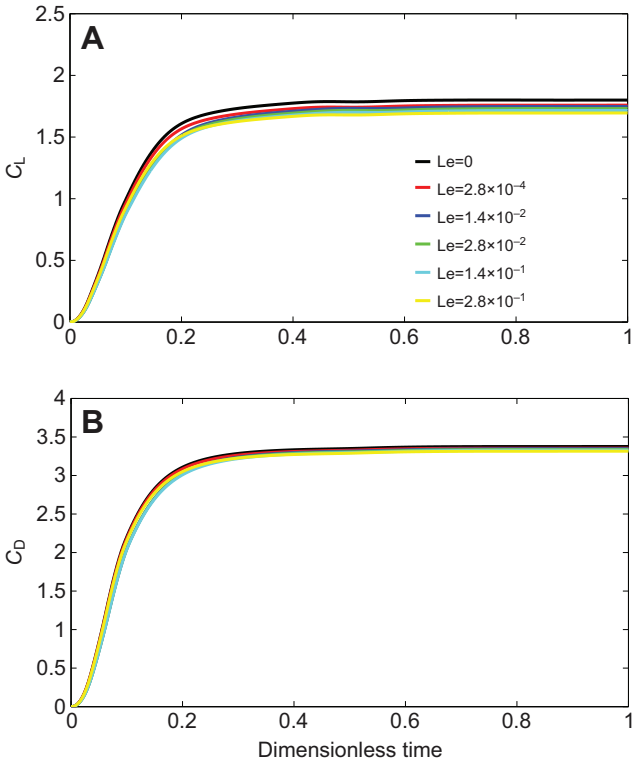

Fig. 8. Force coefficients for a single wing in background flow at a 45 deg angle of attack at *Re*=10 for varying values of the porosity. The wing is fixed in place, and the background flow is ramped from zero to the characteristic velocity at time t'=0.2. (A) Lift coefficients as a function of dimensionless time. Maximum lift is achieved when the porosity/leakiness is zero, which is equivalent to a solid wing. (B) Drag coefficients as a function of dimensionless time.

The Journal of Experimental Biology (2014) doi:10.1242/jeb.084897

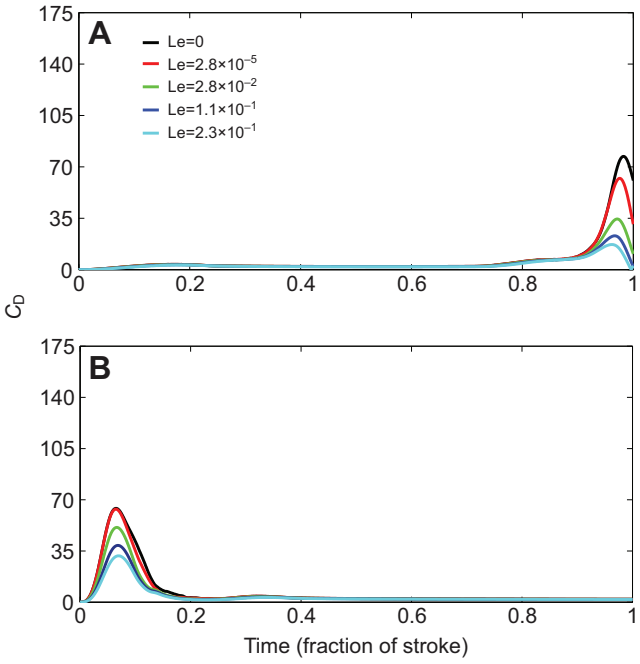

Fig. 9. Drag coefficients as a function of time (fraction of stroke) for *Re*=10. (A) Drag coefficients generated during the clap. Note that Le=0 corresponds to a solid wing. The peaks in the drag coefficients at the end of the stroke correspond to the large forces required to clap the wings together at low *Re*. (B) Drag coefficients generated during fling. The initial large peak in the drag coefficients corresponds to the large forces required to fling the wings apart in a viscous fluid. The peak drag force is reduced for the porous case compared with the solid case.

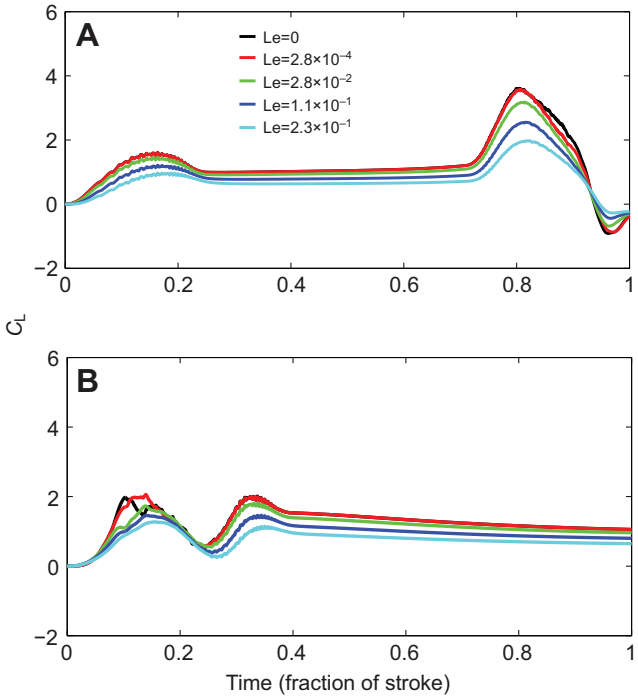

Fig. 10. Lift coefficients as a function of time (fraction of stroke) for *Re*=10. (A) Lift coefficients generated during the clap. The large peaks in the lift coefficients correspond to the augmented lift generated when the wings are clapped together. (B) Lift coefficients generated during the fling. The initial large peaks correspond to the augmented lift generated during the fling. Peak lift is reduced for the porous case, but not as much as the peak drag.

Fig. 10 shows the corresponding lift coefficients as a function of time (fraction of stroke) for *Re*=10. The solid wing case and four leakiness values ranging from 2.8×10^{-4} (least leaky) to 2.3×10^{-1} (most leaky) were examined. During the upstroke, the peak in the lift coefficients at the end of the stroke corresponds to the lift augmentation effect generated by the clap (Fig. 10A). During the downstroke, the initial large peak in the lift coefficients corresponds to the lift-augmenting effect of the fling generated during wing rotation (Fig. 10B). This lift-augmenting effect continues for some time during wing translation. In general, the average and peak lift values are lower for the porous case compared with the solid case, and this effect increases rapidly for Le>2.8×10^{-2}.

Fig. 11 shows the drag coefficients as a function of time (fraction of stroke) for *Re*=4. The dimensionless porosities examined were the same as in Fig. 9. During the clap, the wings initially accelerate towards each other, and then the forces plateau until the effect of the other wing is felt. Towards the end of the stroke, the wings begin to rotate and clap together. The large peak in the drag coefficients corresponds to the force required to clap the wings together (Fig. 11A). During the fling, the initial large peaks correspond to the forces required to rapidly fling the wings apart (Fig. 11B). The drag coefficients then plateau as the wings translate apart. The peak drag is lowered for the porous cases compared with the corresponding solid cases. The reduction in peak drag is perceived more for the *Re*=4 case than for *Re*=10.

Snapshots of the vorticity fields with velocity vectors are shown in Fig. 12 for fling at *Re*=10 for a solid wing (Le=0) and a porous wing (Le=2.3×10^{-1}). The vorticity and velocity fields are very similar with and without the addition of porosity. During the clap (not shown), a strong downward jet is generated between the wings that is responsible for some lift augmentation. During the fling, two large leading edge vortices are formed, and no trailing edge vortices are formed initially. This vortical asymmetry (strong leading edge vortices and weak trailing edge vortices) increases the circulation about the wings and augments the lift generated. The leading and trailing edge vortices are more diffuse for the porous case, but the basic flow patterns are the same.

Effect of initial gap width between wings

Fig. 13 shows the lift and drag coefficients as a function of time (fraction of stroke) during a fling for *Re*=10 and Le=2.3×10^{-1}. The initial gap width between the centers of the wings was varied from 1/2 to 1/10 chord lengths. The large peaks in the force coefficients correspond to forces required to fling the wings apart. The peak drag forces continue to decrease as the initial gap between the wings is increased. Changes in the peak lift force generated were small in comparison to the drag forces.

Average and peak forces

Peak drag coefficients generated during the fling are shown in Fig. 14 as functions of *Re*. While decreasing *Re* increases the peak drag coefficient, the inclusion of wing leakiness decreases this value for a particular *Re*. For leakiness values relevant to thrips (Le>0.15), the reduction in peak drag is of the order of 50% or more. The scaled porosity was set to 0 (for the case of the solid wing), 2×10^{-5}, 2×10^{-3}, 8×10^{-3} and 16×10^{-3}. Note that the peak drag coefficients for the solid wing cases are an order of magnitude larger than the forces required to translate a single wing. Decreasing *Re* increases the peak drag coefficient from ~90 at *Re*=10 to ~160 at *Re*=4. The inclusion

The Journal of Experimental Biology (2014) doi:10.1242/jeb.084897

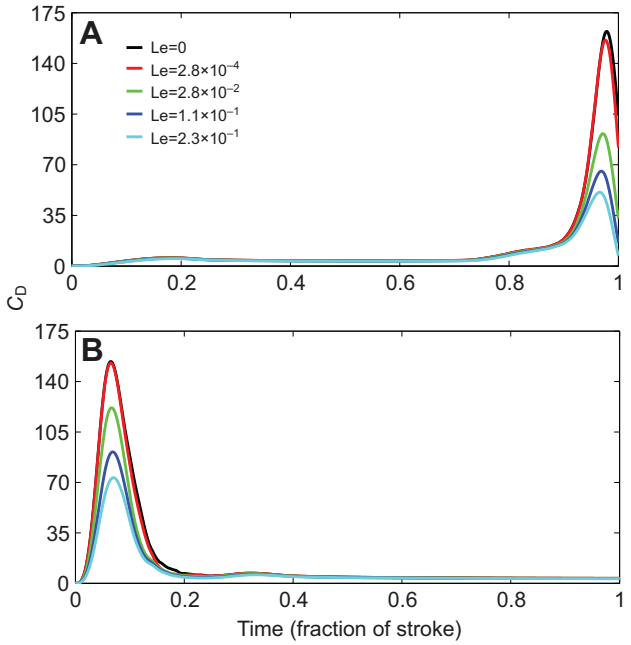

Fig. 11. Drag coefficients as a function of time (fraction of stroke) for *Re*=4. (A) Drag coefficients generated during the clap. The large peaks in the drag coefficients correspond to the force required to clap the wings together. (B) Drag coefficients generated during the fling. The initial large peaks correspond to the forces required to rapidly fling the wings apart. The peak drag forces are lowered for the porous cases compared with the corresponding solid cases.

of wing porosity decreases the peak drag coefficient for each *Re*. The reduction in drag is significant for $\lambda>10^{-4}$.

The average lift to drag ratios calculated during the fling downstroke are shown in Fig. 15 as functions of the leakiness, Le. The *Re* was set to 10, 8, 6 and 4. Fig. 15A shows that average lift over the entire downstroke is maximized for the case of a solid wing (Le=0) for all Reynolds numbers. The average lift slowly decreases until $Le\approx5.0\times10^{-2}$ and then lift begins to quickly decrease for $Le>5.0\times10^{-2}$. Average drag over the entire downstroke is also highest for the case of the solid wing (Le=0) and increases with decreasing *Re*. The average drag also decreases with increasing leakiness. Lift over drag is maximized when Le is set to about 7.5×10^{-2} for all *Re* (Fig. 15C). In these cases, the large peaks in drag generated as the wings are brought together are substantially reduced, but the lift coefficients are not significantly decreased.

DISCUSSION

As a result of many experimental, computational and theoretical studies, much is known about the aerodynamic mechanisms that generate lift in larger insects (Dickinson et al., 1999; Ellington, 1999; Liu et al., 1998; Ramamutri and Sandberg, 2002; Birch and Dickinson, 2003; Mao and Wu, 2003; Usherwood, 2003). Insect aerodynamics are fundamentally different, however, at the lowest *Re* observed for insects because of the significant viscous effects that characterize these flows. Computational work shows that at lower *Re*, the leading and trailing edge vortices remain attached to single wings during translation, resulting in reduced lift coefficients and increased drag coefficients (Miller and Peskin, 2004). An aerodynamic feature observed in the flight of small insects that might compensate for this loss of lift is the predominant use of clap and fling (Ellington, 1999; Dudley, 2000). Numerical simulations suggest that the clap and fling mechanism works best in terms of lift production at lower *Re*, so it is perhaps not surprising that most tiny insects use it (Miller and Peskin, 2005; Miller and Peskin, 2009). What has been largely ignored in most analytical and numerical studies, however, is the very large drag forces that are generated during the clap and fling at lower *Re*. Results from a computational study by Miller and Peskin (Miller and Peskin, 2009) suggest that flexibility reduces the large drag forces generated during clap and fling while maintaining lift for a certain range of wing flexibilities. However, the drag forces generated for during clap and fling are still 3–5 times greater than during single wing translation for biologically realistic flexibilities.

In this paper, the role of bristled wing structures was explored as another mechanism to reduce the drag required to clap together and fling apart wings at lower *Re*. Although it has been suggested that this wing design enhances flight performance at low *Re*, no experimental or computational study has supported this claim. In fact, Sunada et al. (Sunada et al., 2002) found no aerodynamic benefit when they compared lift and drag coefficients generated in physical models of fringed and solid wings at a Reynolds number of 10. When wing–wing interactions are considered, however, the highest lift over drag ratios are found for leakiness values of about $Le=7.5\times10^{-2}$. This is primarily due to the reduced cost of rapidly flapping together and flinging apart porous wings in a viscous fluid. It has been shown previously in experiments with physical models that the movement of bristles near a boundary increases the flow between the bristles (Loudon et al., 1994). Similarly, the motion of two wings in close proximity can also increase the flow between the bristles and reduce the drag forces acting on each structure.

The relevant range of dimensionless porosities or leakiness for thrips wings is 0.15–0.28. These values are beyond the range where lift over drag is optimized, suggesting that the bristles reduce the total force required to clap the wings together and fling them apart rather than augmenting lift or lift over drag. As the majority of the forces acting on each wing during the end of the clap and the beginning of the fling are in opposite directions and cancel, it seems reasonable to reduce this force so as to decrease both the cost and peak force requirements for flight. As the lift and drag forces are reduced proportionally, the changes in lift over drag are modest for biologically relevant ranges of porosity.

Possible rarefied effects

At the scale of flow between each individual bristle, the continuum assumption for the fluid may introduce errors (Liu and Aono, 2009). The Knudsen number, *Kn*, gives a measure of the mean free path of a molecule over the characteristic length scale and is given by the equation:

$$Kn=\frac{k_{\mathrm{B}}T}{\sqrt{2}\pi\sigma^{2}pL}=\frac{\lambda}{\tilde{L}}, \qquad (11)$$

where k_{B} is the Boltzmann constant, T is the thermodynamic temperature, p is the total pressure, σ is the particle hard shell diameter, λ is the mean free path and $\tilde{L}$ is the characteristic length scale. In this case, $\tilde{L}$ is the length between bristles. Assuming that thrips bristles are 2 μm in diameter with a 20 μm gap (Ellington, 1980), and standard temperature and pressure, the Knudsen number is about 0.004. Fluids are well described by continuum laws for $Kn<0.001$. For $0.001<Kn<1$, the no-slip condition is violated, and these effects may be accounted for by increasing the amount of slip between the boundary and the fluid (Dyson et al., 2008), and this may be done in the simulations by increasing the leakiness.

The Journal of Experimental Biology (2014) doi:10.1242/jeb.084897

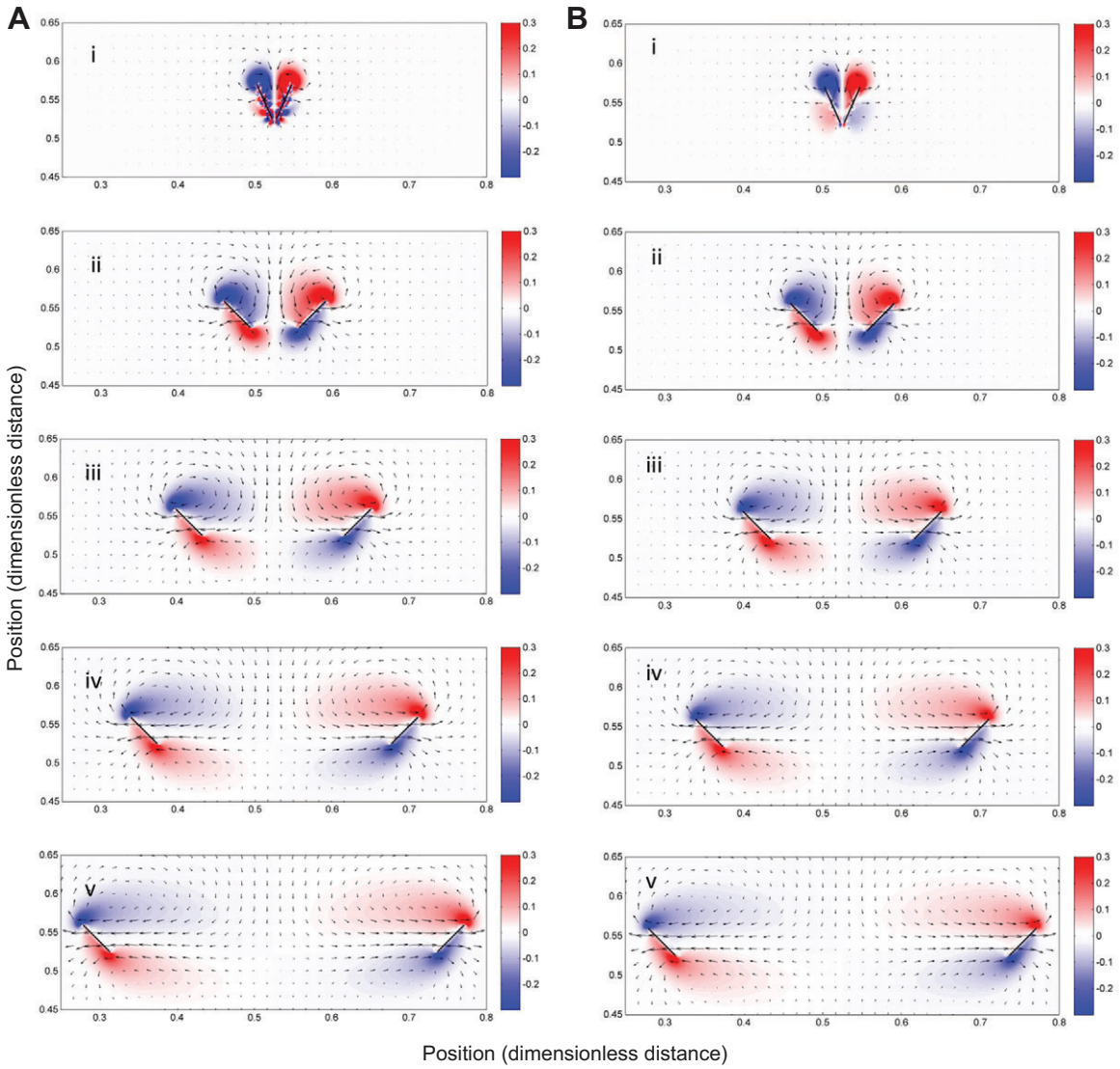

Fig. 12. Snapshots of the vorticity fields with velocity vectors for the fling at *Re*=10. i–v represent a snapshot in time taken at 20%, 40%, 60%, 80% and 100% of the half stroke. (A) A solid wing (Le=0) and (B) a porous wing (Le=2.3×10^{-1}). During the fling, two large leading edge vortices are formed that enhance the lift acting on each wing. The larger leading edge vortices remain for some time as the wings translate apart. The vorticity and velocity fields for the porous and solid wings are not substantially different, but the magnitude of vorticity is slightly decreased for the porous case.

Intermittent parachuting as a dispersal mechanism

This paper also presents the first analysis of the wing motion of a tiny insect with bristled wings. The clap and fling motion was observed for all individuals, although the wings did not come close enough to touch during the clap. We also obtained some of the first footage of a passive parachuting mechanism being employed by the smallest flying insects. Although we were not able to track the thrips for long periods of flight, the footage does suggest that thrips may alternate between passive and active flight modes as they disperse over distances of miles. The advantage here is that periods of passive flight could conserve significant amounts of energy during long distance dispersal. Longer distance tracking studies are needed, however, to verify this claim.

MATERIALS AND METHODS

Video recordings of free-flying tiny insects

Thrips were collected in Chapel Hill, NC, USA, during late July to early August, 2009 from daylilies and gardenia flowers. The insects and flowers were brought to the lab and filmed within 8 h of collection. A pipette tip was placed over the thrips to allow them to crawl on to the inner surface of the tip. The pipette was then suspended upside down in the field of view of the cameras so that the thrips could crawl down the tube and take-off from the tip.

Two high-speed cameras (Phantom v7.1, Vision Research, Wayne, NJ, USA) were each equipped with a 55 mm micro-Nikkor lens and 27.5 mm extension tube and arranged perpendicularly for stereo filming (see Fig. 16). Magnifying lenses were used to aim the beams from halogen bulbs directly into the camera apertures. The thrips were filmed at 4000 frames s^{-1} with a 15–30 µs exposure time. The cameras were calibrated by waving a wand of known dimension in the field of view. Calibration and analysis of the wing motion was performed using DLTdv5 software (Hedrick, 2008) with additional custom-written routines to perform the structure-from-motion wand-wave calibration. DLTdv5 is a digitizing environment written in MATLAB designed to acquire 3D coordinates from multiple video sources calibrated via a set of direct linear transformation (DLT) coefficients. Recording of the thrips began when they were observed to prepare for flight by raising their wings.

Computational method

The immersed boundary method (Peskin, 2002) was used to solve the fully coupled fluid–structure interaction problem of two porous wings performing

The Journal of Experimental Biology (2014) doi:10.1242/jeb.084897

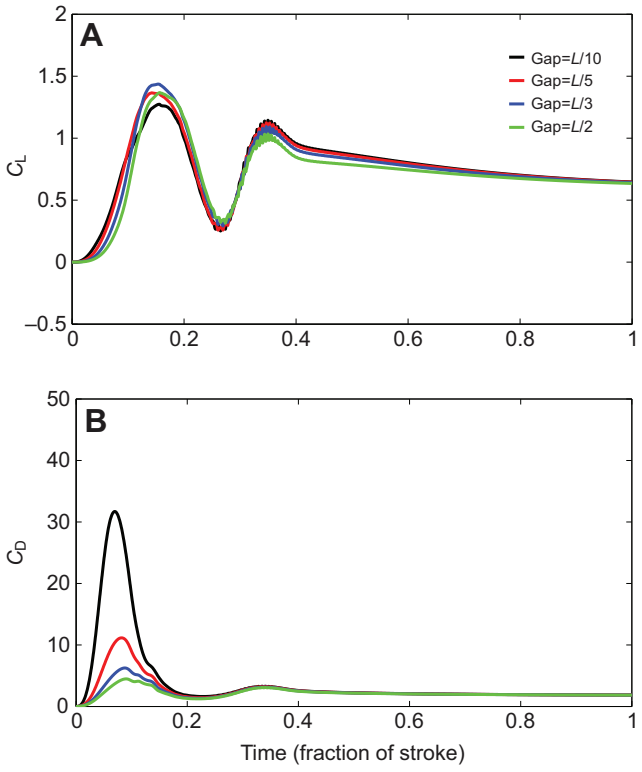

Fig. 13. Lift and drag coefficients as a function of time (fraction of stroke) during a fling for *Re*=10, Le=2.3×10^{-1}, and varying initial gap widths between the wings as a fraction of the chord length, *L*. (A) Lift coefficients and (B) drag coefficients. The large peaks in the force coefficients correspond to forces required to fling the wings apart. The peak drag forces continue to decrease as the initial gap between the wings is increased.

a clap and a fling. The full Navier–Stokes equations were solved on a fixed Cartesian grid, and the elastic boundary equations were discretized on a moving Lagrangian grid. The immersed boundary method provides an efficient way of handling the interaction between these two grids.

A description of the two-dimensional, non-porous immersed boundary method is given below. The equations of fluid motion are the incompressible Navier–Stokes equations:

$$\rho\left(\mathbf{u}_t(\mathbf{x},t)+\mathbf{u}(\mathbf{x},t)\cdot\nabla\mathbf{u}(\mathbf{x},t)\right)=\nabla p(\mathbf{x},t)+\mu\Delta\mathbf{u}(\mathbf{x},t)+\mathbf{f}(\mathbf{x},t)\,, \quad (12)$$

$$\nabla\cdot\mathbf{u}(\mathbf{x},t)=0\,, \quad (13)$$

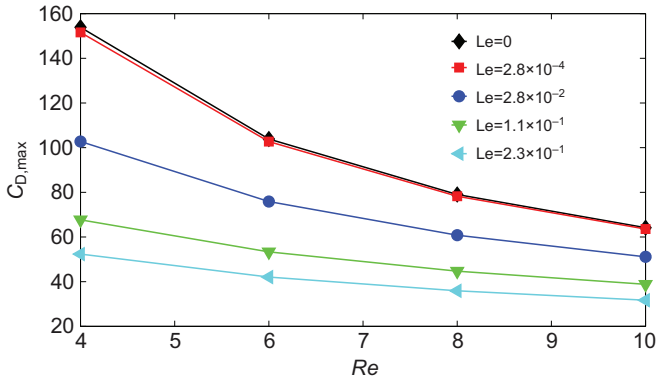

Fig. 14. Peak drag coefficient ($C_{D,max}$) during a fling as a function of *Re*. While decreasing *Re* increases the peak drag coefficient, the inclusion of wing leakiness decreases this value for a particular *Re*. For leakiness values relevant to thrips (Le>0.15), the reduction in peak drag is of the order of 50% or more.

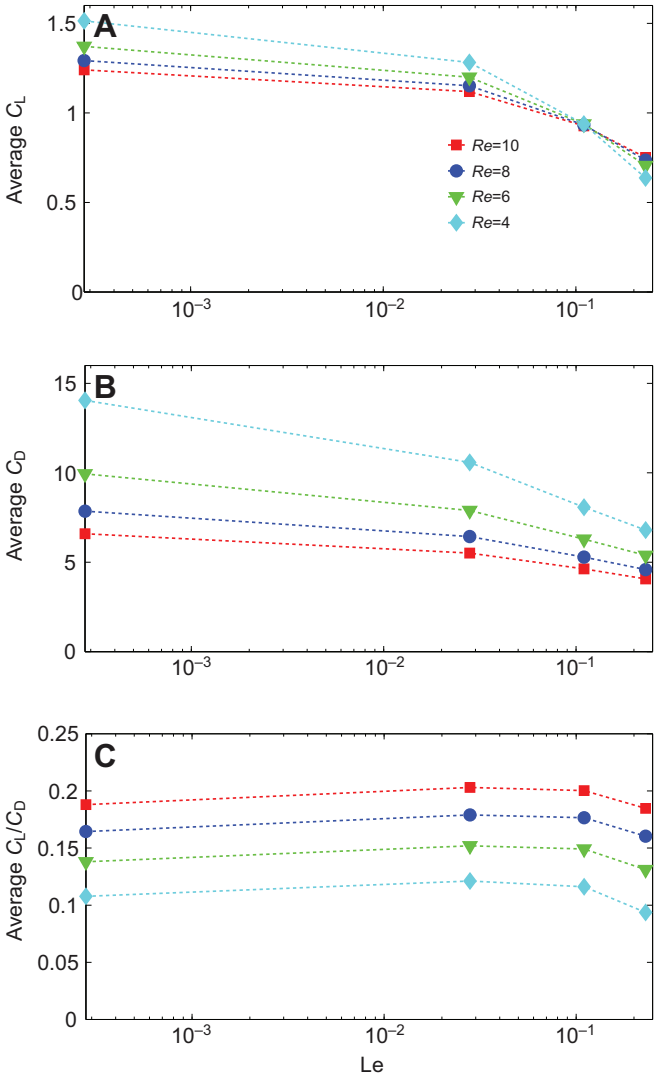

Fig. 15. Average lift and drag ratios during the entire downstroke as a function of the leakiness Le for *Re*=10, 8, 6 and 4. (A) Average lift over the entire downstroke is maximized for the case of a solid wing (Le=0). Average lift slowly decreases until Le≈5.0×10^{-2}and then lift begins to quickly decrease. (B) Average drag over the entire downstroke is highest for the case of the solid wing (Le=0) and decreases with increasing leakiness. (C) Lift over drag is maximized when Le is set to about 7.5×10^{-2}. For this case, the large peak in drag generated as the wings are brought together is substantially reduced, but the lift coefficients are not significantly decreased.

where $\mathbf{u}(\mathbf{x},t)$ is the fluid velocity at Cartesian coordinate $\mathbf{x}$ and time t, $p(\mathbf{x},t)$ is the pressure and $\mathbf{f}(\mathbf{x},t)$ is the force per unit area acting on the fluid. The interaction between the fluid and the boundary is given by the following equations:

$$\mathbf{f}(\mathbf{x},t)=\int\mathbf{F}(q,t)\delta\left(\mathbf{x}-\mathbf{X}(q,t)\right)\mathrm{d}q\,, \quad (14)$$

$$\mathbf{X}_t(q,t)=\mathbf{U}\left(\mathbf{X}(q,t)\right)=\int\mathbf{u}(\mathbf{x},t)\delta\left(\mathbf{x}-\mathbf{X}(q,t)\right)\mathrm{d}\mathbf{x}\,, \quad (15)$$

where $\delta(\mathbf{x})$ is a 2D delta function. Eqn 14 applies force from the boundary to the fluid grid, and Eqn 15 evaluates the local fluid velocity at the boundary. The boundary is then moved at the local fluid velocity, and this enforces the no-slip condition. The exact discretization used in these simulations has been described elsewhere (Peskin and McQueen, 1996; Miller and Peskin, 2009).

The force $\mathbf{F}(q,t)$ is specific to the problem. Boundaries have been modeled in the immersed boundary framework that include active elastic forces due to muscle contraction (Peskin and McQueen, 1996), cohesive forces

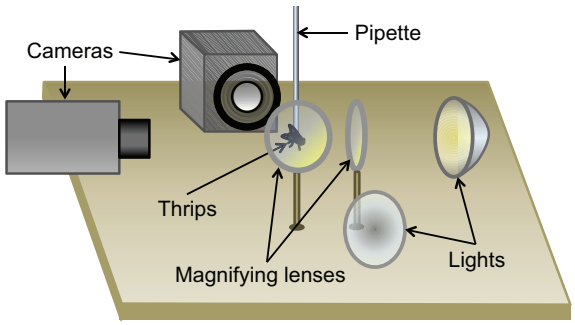

Fig. 16. Diagram of the experimental setup. Diagram not to scale. Thrips were filmed in stereo using two high-speed cameras operating at 4000 frames s^{-1} with a shutter duration of 15–30 µs. Lighting was provided by 300 W halogen bulbs positioned such that the beam of light was focused directly on the camera aperture using a magnifying lens. The cameras were focused on a pipette tip, which held the thrips; recordings were collected as the thrips emerged from the pipette tip and flew away.

between boundaries or cells (Fogelson and Guy, 2008), and the action of dynein molecular motors (Dillon et al., 2007). In a simple case where boundary points are tethered to target points, the equation describing the force applied to the fluid by the boundary is:

$$\mathbf{F}(q,t) = k_{\text{targ}}\left(\mathbf{Y}(q,t) - \mathbf{X}(q,t)\right), \quad (16)$$

where k_{targ} is a stiffness coefficient and $\mathbf{Y}(q,t)$ is the prescribed position of the target boundary.

Acknowledgements
The authors would like to thank Charles Peskin for advice on the porous immersed boundary method and William Kier for insightful discussions on working with invertebrates.

Competing interests
The authors declare no competing financial interests.

Author contributions
The initial concept for modelling bristled wings as porous boundaries was made my L.A.M., and the initial concept for filming thrips was made by T.L.H. Simulations were designed by L.A.M. and performed and analysed by A.S. The design of the flight recordings was by T.L.H., and the thrips were filmed by A.K.R. Flight kinematics were analysed by A.A.L., S.G. and S.J. The manuscript was written by A.S., L.A.M. and T.L.H.

Funding
This research was supported by the Burroughs Wellcome Fund (CASI award ID no. 1005782.01) and the National Science Foundation (NSF; DMS FRG 0854961) to L.A.M. and NSF IOS-0920358 to T.L.H.

Supplementary material
Supplementary material available online at
http://jeb.biologists.org/lookup/suppl/doi:10.1242/jeb.084897/-/DC1

References
Alexander, M. R. (2003). *Principles of Animal Locomotion*. Princeton, NJ: Princeton University Press.
Austin, A. and Dowton, M. (2000). *Hymenoptera: Evolution, Biodiversity and Biological Control*. Collingwood: Csiro Publishing.
Bennett, L. (1977). Clap and fling aerodynamics – an experimental evaluation. *J. Exp. Biol.* **69**, 261-272.
Birch, J. M. and Dickinson, M. H. (2003). The influence of wing-wake interactions on the production of aerodynamic forces in flapping flight. *J. Exp. Biol.* **206**, 2257-2272.
Birch, J. M., Dickson, W. B. and Dickinson, M. H. (2004). Force production and flow structure of the leading edge vortex on flapping wings at high and low Reynolds numbers. *J. Exp. Biol.* **207**, 1063-1072.
Bringley, T. T. and Peskin, C. S. (2008). Validation of a simple method for representing spheres and slender bodies in an immersed boundary method for Stokes flow on an unbounded domain. *J. Comput. Phys.* **227**, 5397-5425.
Cheer, A. Y. L. and Koehl, M. A. R. (1987). Paddles and rakes: fluid flow through bristled appendages of small organisms. *J. Theor. Biol.* **129**, 17-39.
Crespi, B. J., Carmean, D. A. and Chapman, T. W. (1997). Ecology and evolution of galling thrips and their allies. *Annu. Rev. Entomol.* **42**, 51-71.
Dickinson, M. H. and Götz, K. G. (1993). Unsteady aerodynamic performance of model wings at low Reynolds numbers. *J. Exp. Biol.* **174**, 45-64.
Dickinson, M. H., Lehmann, F. O. and Sane, S. P. (1999). Wing rotation and the aerodynamic basis of insect flight. *Science* **284**, 1954-1960.
Dillon, R. H., Fauci, L. J., Omoto, C. and Yang, X. (2007). Fluid dynamic models of flagellar and ciliary beating. *Ann. N. Y. Acad. Sci.* **1101**, 494-505.
Dudley, R. (2000). *The Biomechanics of Insect Flight: Form, Function, Evolution*. Princeton, NJ: Princeton University Press.
Dyson, P., Ransing, R., Williams, P. J. and Williams, R. (2008). *Fluid Properties at Nano/Meso Scale: A Numerical Treatment.* Chichester: John Wiley & Sons Ltd.
Ellington, C. P. (1980). Wing mechanics and take-off preparation of thrips (Thysanoptera). *J. Exp. Biol.* **85**, 129-136.
Ellington, C. P. (1984). The aerodynamics of hovering insect flight. III. Kinematics. *Philos. Trans. R. Soc. B* **305**, 79-113.
Ellington, C. P. (1999). The novel aerodynamics of insect flight: applications to micro-air vehicles. *J. Exp. Biol.* **202**, 3439-3448.
Ellington, C. P., van den Berg, C., Willmont, A. P. and Thomas, A. L. R. (1996). Leading edge vortices in insect flight. *Nature* **348**, 626-630.
Fogelson, A. L. and Guy, R. D. (2008). Immersed-boundary-motivated models of intravascular platelet aggregation. *Comput. Methods Appl. Mech. Eng.* **197**, 2087-2104.
Hedrick, T. L. (2008). Software techniques for two- and three-dimensional kinematic measurements of biological and biomimetic systems. *Bioinspir. Biomim.* **3**, 034001.
Hedrick, T. L., Cheng, B. and Deng, X. (2009). Wingbeat time and the scaling of passive rotational damping in flapping flight. *Science* **324**, 252-255.
Horridge, G. A. (1956). The flight of very small insects. *Nature* **178**, 1334-1335.
Wang, Z. J. (2000). Two dimensional mechanism for insect hovering. *Phys. Rev. Lett.* **85**, 2216-2219.
Jones, D. R. (2005). Plant viruses transmitted by thrips. *Eur. J. Plant Pathol.* **113**, 119-157.
Kim, Y. and Peskin, C. S. (2006). 2-D parachute simulation by the immersed boundary method. *SIAM J. Sci. Comput.* **28**, 2294-2312.
Kolomenskiy, D., Moffatt, H. K., Farge, M. and Schneider, K. (2010). Vorticity generation during the clap-fling-sweep of some hovering insects. *Theor. Comput. Fluid Dyn.* **24**, 209-215.
Kolomenskiy, D., Moffatt, H. K., Farge, M. and Schneider, K. (2011). Two- and three-dimensional numerical simulations of the clap–fling–sweep of hovering insects. *J. Fluids Structures* **27**, 784-791.
Lewis, T. (1964). The weather and mass flights of Thysanoptera. *Ann. Appl. Biol.* **53**, 165-170.
Lewis, T. (1965). The species, aerial density and sexual maturity of Thysanoptera caught in mass flights. *Ann. Appl. Biol.* **55**, 219-225.
Lighthill, M. J. (1973). On the Weis-Fogh mechanism of lift generation. *J. Fluid Mech.* **60**, 1-17.
Liu, H. and Aono, H. (2009). Size effects on insect hovering aerodynamics: an integrated computation study. *Bioinspir. Biomim.* **4**, 015002.
Liu, H., Ellington, C., Kawachi, K., van den Berg, C. and Willmott, A. P. (1998). A computational fluid dynamic study of hawkmoth hovering. *J. Exp. Biol.* **201**, 461-477.
Loudon, C., Best, B. and Koehl, M. (1994). When does motion relative to neighboring surfaces alter the flow through arrays of hairs? *J. Exp. Biol.* **193**, 233-254.
Maxworthy, T. (1979). Experiments on the Weis-Fogh mechanism of lift generation by insects in hovering flight. Part I. Dynamics of the 'fling'. *J. Fluid Mech.* **93**, 47-63.
Miller, L. A. and Peskin, C. S. (2004). When vortices stick: an aerodynamic transition in tiny insect flight. *J. Exp. Biol.* **207**, 3073-3088.
Miller, L. A. and Peskin, C. S. (2005). A computational fluid dynamics of 'clap and fling' in the smallest insects. *J. Exp. Biol.* **208**, 195-212.
Miller, L. A. and Peskin, C. S. (2009). Flexible clap and fling in tiny insect flight. *J. Exp. Biol.* **212**, 3076-3090.
Miller, L. A., Santhanakrishnan, A., Jones, S., Hamlet, C., Mertens, K. and Zhu, L. (2012). Reconfiguration and the reduction of vortex-induced vibrations in broad leaves. *J. Exp. Biol.* **215**, 2716-2727.
Morse, J. G. and Hoddle, M. S. (2006). Invasion biology of thrips. *Annu. Rev. Entomol.* **51**, 67-89.
Palmer, J. M., Reddy, D. V. R., Wightman, J. A. and Ranga Rao, G. V. (1990). New information on the thrips vectors of tomato spotted wilt virus in groundnut crops in India. *International Arachis Newsletter* **7**, 24-25.
Peskin, C. S. (2002). The immersed boundary method. *Acta Numerica* **11**, 479-517.
Peskin, C. S. and McQueen, D. M. (1996). Fluid dynamics of the heart and its valves. In *Case Studies in Mathematical Modeling: Ecology, Physiology, and Cell Biology*, 2nd edn (ed. H. G. Othmer, F. R. Adler, M. A. Lewis and J. C. Dallon), pp. 309-337. Englewood Cliffs, NJ: Prentice-Hall.
Ramamutri, R. and Sandberg, W. C. (2002). A three-dimensional computational study of the aerodynamic mechanisms of insect flight. *J. Exp. Biol.* **205**, 2997-3008.
Spedding, G. R. and Maxworthy, T. (1986). The generation of circulation and lift in a rigid two-dimensional fling. *J. Fluid Mech.* **165**, 247-272.
Srygley, R. B. and Thomas, A. L. R. (2002). Unconventional lift-generating mechanisms in free-flying butterflies. *Nature* **420**, 660-664.
Stockie, J. M. (2009). Modelling and simulation of porous immersed boundaries. *Comput. Struct.* **87**, 701-709.
Mao, S. and Wu, J. H. (2003). Aerodynamic force generation and power requirements in forward flight in a fruit fly with modeled wing motion. *J. Exp. Biol.* **206**, 3065-3083.

Mao, S. and Xin, Y. (2003). Flow around two airfoils performing fling and subsequent translation and translation and subsequent flap. *Acta Mech. Sin.* **19**, 103-117.
Sunada, S., Takashima, H., Hattori, T., Yasuda, K. and Kawachi, K. (2002). Fluid-dynamic characteristics of a bristled wing. *J. Exp. Biol.* **205**, 2737-2744.
Terry, I. (2001). Thrips and weevils as dual, specialist pollinators of the Australian Cycad *Macrozamia communis* (Zamiaceae). *Int. J. Plant Sci.* **162**, 1293-1305.
Terry, I. (2002). Thrips: the primeval pollinators? In *Thrips And Tospoviruses: Proceedings of The 7th International Symposium on Thysanoptera* (ed. L. Mound and R. Marullo), pp. 157-162. Canberra: Australian National Insect Collection CSIRO.
Ullman, D. E., Meideros, R., Campbell, L. R., Whitfield, A. E., Sherwood, J. L. and German, T. L. (2002). Thrips as vectors of tospoviruses. *Adv. Bot. Res.* **36**, 113-140.
Usherwood, J. (2003). More than a flitting tour of flapping flight: the biomechanics of insect flight. *J. Exp. Biol.* **206**, 2095-2096.
Usherwood, J. R. and Ellington, C. P. (2002). The aerodynamics of revolving wings I. Model hawkmoth wings. *J. Exp. Biol.* **205**, 1547-1564.
van den Berg, C. and Ellington, C. P. (1997a). The three-dimensional leading-edge vortex of a 'hovering' model hawkmoth. *Philos. Trans. R. Soc. B* **352**, 329-340.
van den Berg, C. and Ellington, C. P. (1997b). The vortex wake of a 'hovering' model hawkmoth. *Philos. Trans. R. Soc. B* **352**, 317-328.
Vogel, S. (1962). A possible role of the boundary layer in insect flight. *Nature* **193**, 1201-1202.
Vogel, S. (1967). Flight in *Drosophila*. II. Variations in stroke parameters and wing contour. *J. Exp. Biol.* **46**, 383-392.
Wang, Z. J. (2000). *Two dimensional mechanism for insect hovering. Phys. Rev. Lett.* **85**, 2216-2219.
Wang, Z. J. (2005). Dissecting insect flight. *Annu. Rev. Fluid Mech.* **37**, 183-210.
Weis-Fogh, T. (1973). Quick estimates of flight fitness in hovering animals, including novel mechanisms for lift production. *J. Exp. Biol.* **59**, 169-230.
Weis-Fogh, T. (1975). Unusual mechanisms for the generation of lift in flying animals. *Sci. Am.* **233**, 81-87.
Wu, J. H. and Mao, S. (2004). Unsteady aerodynamic forces of a flapping wing. *J. Exp. Biol.* **207**, 1137-1150.